# Simulating a Syringe Behaviour Using a Pneumatic Cylinder Haptic Interface

Thibault Senac, Arnaud Lelevé, Richard Moreau, Laurent Krähenbühl,

Florent Sigwalt, Christian Bauer

# Simulating a Syringe Behaviour Using a Pneumatic Cylinder Haptic Interface

Thibault Senac, Arnaud Lelevé, Richard Moreau, Laurent Krähenbühl,
Florent Sigwalt, Christian Bauer

HAL Id: hal-02176436

https://hal.archives-ouvertes.fr/hal-02176436

Submitted on 12 Sep 2019

# Simulating a Syringe Behaviour Using a Pneumatic Cylinder Haptic Interface

T. Sénac[a,*], A. Lelevé[a], R. Moreau, L. Krahenbuhl[a], F. Sigwalt[b], C. Bauer[b,c]

[a]*University of Lyon, INSA Lyon, École Centrale de Lyon, CNRS, Ampère, F-69621, Villeurbanne, France*
[b]*Département d'Anesthésie-Réanimation, Hôpital de la Croix Rousse, Hospices Civils de Lyon, Lyon, France*
[c]*Centre Lyonnais d'Enseignement par la Simulation en Santé, SAMSEI, Université Claude Bernard Lyon 1, Lyon, France*

## Abstract

Mastering medical gestures, such as epidural needle insertion, requires much practice. Haptic interfaces can be efficient training solutions. Nevertheless, they must provide users with an accurate experience for an effective training. This article introduces a control framework that turns a pneumatic cylinder into a haptic interface able to simulate a syringe and more specifically the loss of resistance phenomenon encountered during an epidural needle insertion. To achieve this, the framework switches between two control laws (position and force tracking) according to the system state. Experiments involving two anesthetists confirm the practicality of this system for hands-on training or rehearsal purposes.

*Keywords:* Haptic Interface, Pneumatic Control, Epidural Anesthesia, Backstepping Control, Switched Systems

## 1. Introduction

Medical gestures usually require much practice in order to properly master them. For instance, the epidural anesthesia gesture learning requires around 90 attempts to reach only an 80% success rate [1]. However, from an ethical point of view, it is desirable to "never do [these attempts] the first time on a patient" as stated by the *Haute Autorité de la Santé* [2] which is the authority in charge of healthcare issues in France. This new constraint raises the need for a simulated training environment using manikins for example. As Vaughan *et al.* [1] and Coles *et al.* [3] point out, using computer driven haptic simulators for this purpose may provide a powerful and efficient training solution in terms of supervision, customization of the training cases and skill assessment.

In this context, one needs to replicate a realistic epidural anesthesia procedure in order to provide an efficient training tool for this particular medical gesture. This procedure consists in introducing a needle into the epidural space in the spinal column in order to inject an anesthetic product into it. The difficulty of this gesture is the localization of the epidural space and stopping the insertion as soon as the tip of the needle enters it. As the haptic feedback from the needle is not precise enough to tell it, anesthetists plug a syringe full of saline liquid onto the needle and constantly push on the plunger flange in order to maintain some pressure in the syringe and the needle (Fig. 1). As long as the needle tip does not reach the epidural space, the liquid remains inside the needle (or a very small leak of liquid in the crossed tissues may

happen). As soon as the tip of the needle enters the epidural space, the liquid naturally fills it and the pressure in the syringe quickly decreases. This decrease is felt by the user as the signal to promptly stop the insertion of the needle. This brutal decrease of pressure is called "loss of resistance" (LOR) phenomenon. More precisely, in a real case, the resistance force, both in the syringe and on the needle, progressively increases while crossing the ligaments until it reaches a peak in the ligamentum flavum and then plummets: this is the LOR phenomenon as described in [4]. In case the user continues the needle motion, he may create a breach in the dura mater which may be dangerous for the patient.

To emulate this procedure it is necessary to replicate the insertion of a needle into tissues as well as this LOR principle. Moreover, N. Vaughan *et al.* [1] identified the emulation of the LOR *felt on the syringe* as one of the essential components of their ideal epidural anesthesia simulator. In that respect, being able to generate a large spectrum of resistant force would be an essential asset. It is therefore necessary to reproduce a syringe part and a needle insertion part. To replicate the syringe, a 1 degree-of-freedom (DOF) haptic interface was needed. It required to be mounted on another haptic interface only in charge of the needle insertion simulation. This paper only focuses on the syringe part of the simulation.

Some solutions provide training tools to help trainees learn the epidural anesthesia (Manoharan *et al.* [5], Magill *et al.* [6], Dubey *et al.* [7] or Thao *et al.* [8], for example). Furthermore, Vaughan *et al.* [1] analyzed most of the solutions available in 2013. However, the existing solutions only provide a simplified experience when it comes to the LOR emulation. Most of the simulators featuring it use a solenoid valve connected to a real syringe. During the

---
*corresponding author
*Email address:* thibault.senac@ec-lyon.fr (T. Sénac)

Figure 1: Epidural anesthesia procedure and finger position on the LOR syringe

procedure the valve simply opens itself to reproduce the LOR phenomenon. It is an effective and simple solution but it does not provide a wide range of experiences. For instance, it cannot smooth the transition between the resistant and non-resistant points, nor can it modify the force levels produced by the interface.

The simulator part introduced in this paper (visible in right picture of Fig. 2) aims at tackling this particular issue, improving the way LOR is emulated through the syringe. To obtain an overall view, the whole simulator is introduced in the left picture of Fig. 2. The complete simulator will use the position information of the needle tip (available from the other haptic device) to determine which tissue the needle is virtually crossing and set the value of both the needle insertion and syringe emptying resistant forces accordingly. Each patient is represented by a set of parameters: the depth of the derma and width of the ligaments the needle should cross, the magnitude of the resistance force on the syringe plunger in each area crossed by the virtual needle, and how sudden the LOR is.

To do so, one has to be able to virtually empty a syringe full of a saline solution. According to [4], resistant forces may reach at least 6 N on a porcine cadaver. Therefore, the system was designed to be able to generate around 10 N. The list of requirements for this system was to:

- physically reproduce a real LOR syringe. This represents usually a 50 mm stroke and a 10 mm diameter,

- be as light as possible as it will be mounted on a haptic device to reproduce the needle insertion.

- reproduce a variable resistant force up to 10 N,

- allow the user to "empty" and "refill" the simulated syringe when the LOR point is not reached,

Previously, several control laws were proposed to reproduce a given resistant force $F_d^{hap}$ by means of a pneumatic actuator [9]. Three control laws were tested with the sole purpose of creating the LOR feel. This study showed that a pneumatic cylinder could produce accurate enough haptic cues using a backstepping force control. However, these control laws lacked the opportunity to "empty" the simulated syringe. Whenever the user stopped pushing on

the plunger flange, the latter always retreated in a non-realistic way as the control law still asked to generate a force. To enhance the syringe emulation we needed to implement a strategy for the plunger to remain in place when the user stops pushing on it. To solve this issue, this paper proposes an algorithm which switches between two control laws: on the one hand, to obtain the haptic feel while pushing on the plunger flange, and on the other hand, to keep the plunger in place when the user stops pushing on it. A first solution consisted in using a unique force control, with a null desired force when the user stopped pushing on the plunger. However, this solution was not satisfactory: as the position was not controlled, a small drift of the plunger position appeared.
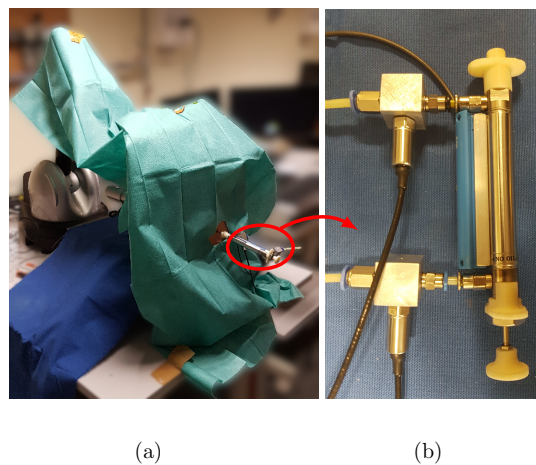


(a)                                    (b)

Figure 2: (a): complete simulator from the point of view of the user, (b): syringe simulator part

This paper uses two distinct control laws to emulate as precisely as possible the syringe behavior during an epidural anesthesia procedure. A supervisory controller is introduced to automatically and safely switch between these low level control laws. The paper is organized as such: section 2 is dedicated to the description of the model and control laws. Section 3 focuses on the switching algorithm. Section 4 provides experimental results.

## 2. Pneumatic Actuator Model and Control

In order to actuate the fake syringe flange, an appropriate actuator (for example electric motors coupled with a pinion and rack, pneumatic cylinders or hydraulic cylinders) had to be selected first. As the required power to mass ratio is high, electric solutions seemed less suitable than pneumatic/hydraulic ones [10]. Moreover regarding the syringe-like desired shape, a cylindrical linear actuator best fits, which is easier to obtain with pneumatic/hydraulic cylinders.

Despite an hydraulic solution seems to be the most obvious choice as it is the closest one to the real system, a

pneumatic cylinder was selected. The pneumatic solution provides high enough forces and allows for an easier maintenance overall (no liquid leaks, for instance). However using pneumatic solutions involves some drawbacks due to the compressibility of air, which increases the complexity of the control. Nevertheless pneumatic actuators have a natural compliance. It allows them to be used in various haptic applications with convincing results as Talhan *et al.*[11] points out, ranging from force feedback gloves [12] to full sized haptic interfaces such as the BirthSIM [13]. The latter example helps obstetricians improve their skills during childbirth delivery.

## 2.1. Pneumatic cylinder model

For this application, a thermodynamical model was used with the A-T transform introduced by Abry *et al.* in [14]. This transform is based on the Park transform [15] and was proposed with a control law for the piston position which used a double effect pneumatic cylinder and two servovalves. In practice, it allows to transform $q_{mN}$ and $q_{mP}$ (the mass flow rates entering into each cylinder chamber) into $q_{mA}$ and $q_{mT}$ (respectively the active and pressuring mass flow rates). Herzig *et al.* [16] have later enhanced this control law by using only one servovalve. The A-T transform provides a convenient way to set up some pneumatic control laws as it permits to directly control the active mass flow rate which directly generates the actuating force. It has been used in previous studies [9, 16] either to design a position control law or to generate haptic feedback. In this model, the friction force is neglected as it is applied on low stiction cylinders, the backlash effect is neglected as the cylinder piston is almost the whole time under charge. Finally, air leakage has been neglected too has its effect was considered as minimal and did not seem to impact too negatively the experimental results in [9]. This model leads to (1):

$$
\begin{cases}
\dfrac{\mathrm{d}y}{\mathrm{d}t} & = \quad v \\
\dfrac{\mathrm{d}v}{\mathrm{d}t} & = \quad \dfrac{-b \cdot v + F_{pneu}}{M} \\
\dfrac{\mathrm{d}F_{pneu}}{\mathrm{d}t} & = \quad -K_{pneu} \cdot v + B_1 \cdot q_{mA} \\
\dfrac{\mathrm{d}K_{pneu}}{\mathrm{d}t} & = \quad \dfrac{f(y, v, K_{pneu}, q_{mA}, q_{mT})}{V_N(y) \cdot V_P(y)}
\end{cases}
\tag{1}
$$

with

$$
\begin{aligned}
f(y, v, K_{pneu}, q_{mA}, q_{mT}) = \\
A_1 \cdot K_{pneu} \cdot y \cdot v - A_2 \cdot F_{pneu} \cdot v \\
-B_2 \cdot y \cdot q_{mA} + B_3 \cdot q_{mT}
\end{aligned}
\tag{2}
$$

where $y$ represents the current position of the piston, $v$ is its velocity, $F_{pneu}$ is the pneumatic force created by the pneumatic cylinder, defined as such:

$$
F_{pneu} = p_P \cdot S_P - p_N \cdot S_N
\tag{3}
$$

Table 1: Variable index.

| Variable | Definition | Unit |
|---|---|---|
| $y$ | piston position | m |
| $\Delta y_{p \to f}$ | distance to switch to force control law | m |
| $\Delta y_{f \to p}$ | distance to switch to position control law | m |
| $v$ | piston velocity | m/s |
| $b$ | pneumatic cylinder physical damping | N.s/m |
| $F_{pneu}$ | pneumatic force | N |
| $M$ | moving parts mass | kg |
| $K_{pneu}$ | pneumatic stiffness | N/m |
| $k$ | polytropic constant | - |
| $r$ | air gas constant | J/(kg.K) |
| $T$ | temperature | K |
| $S$ | cylinder section | m$^2$ |
| $S_N, S_P$ | inner surfaces on each side of the piston | m$^2$ |
| $V_0$ | total cylinder volume | m$^3$ |
| $p_P, p_N$ | pressure in each cylinder chamber | Pa |
| $V_P, V_N$ | volume of each cylinder chamber | m$^3$ |
| $q_{mA}$ | active mass flow rate | kg/s |
| $q_{mT}$ | pressurization mass flow rate | kg/s |
| $q_{mP}, q_{mN}$ | mass flow rates entering each cylinder chamber | kg/s |
| $y_d, v_d, F_d$ | desired position velocity and pneumatic force for position control | - |
| $F_d^{hap}$ | desired pneuamtic force for force control | N |
| $K_{cl}$ | closed loop stiffness | $N/m$ |
| $B_{cl}$ | closed loop damping | $N.s/m$ |
| $t_{del}$ | delay time | $s$ |
| $y_0$ | initial position | $m$ |

3

with $S_N$ and $S_P$ being the inner surfaces on each side of the piston, and $p_P$ and $p_N$ the pressure in each chamber. All these variables are represented in Fig. 3. Moreover, $b$ represents the pneumatic cylinder physical damping, $M$ is the mass of the piston-rod-flange part.

$$A_1 = 2 \cdot S^2 \cdot (k+1) \quad A_2 = S^2 \cdot k \cdot (k+1)$$
$$B_1 = \frac{k \cdot r \cdot T \cdot S}{V_0} \quad B_2 = \frac{S^3 \cdot k^2 \cdot T \cdot r}{V_0}$$
$$B_3 = S^2 \cdot k^2 \cdot T \cdot r$$

are constants where $k$ is the polytropic constant, $r$ the air gas constant, $V_0$ the total pneumatic cylinder volume, $T$ the inner temperature, which is considered constant, and $S$ is the inner cylinder section. $K_{pneu}$ is the pneumatic stiffness defined as follows:

$$K_{pneu} = \left(\frac{p_P}{V_P(y)} + \frac{p_N}{V_N(y)}\right) \cdot k \cdot S^2 \qquad (4)$$

Finally, $q_{mA}$ is the active mass flow rate and $q_{mT}$ the pressurization mas flow rate defined according to the A-T transform [14]. This corresponds to virtual mass flow rates. In this application the use of $q_{mA}$ is sufficient to control either the force produced by the cylinder or the position of the plunger, as Abry *et al.* highlighted in his thesis [17]. Then $q_{mA}$ is defined by:

$$q_{mA} = \frac{V_0}{V_P(y)} \cdot q_{mP} - \frac{V_0}{V_N(y)} \cdot q_{mN} \qquad (5)$$

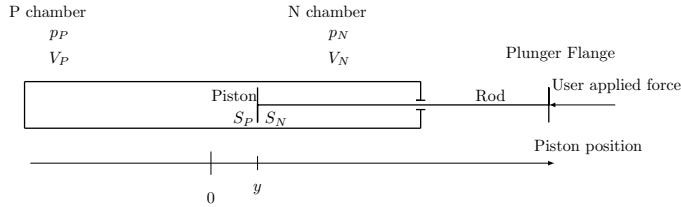Here $V_P$ and $V_N$ are the instantaneous volumes of each



Figure 3: Cylinder diagram.

chamber of the cylinder and can be written $V_P = V_0 + S \cdot y$ and $V_N = V_0 + S \cdot y$. Similarly $q_{mP}$ and $q_{mN}$ are the mass flow rates entering each chamber. To control accurately the 5/2 servovalve[1] which supplies the cylinder chambers, its characterization has been performed in order to get an input-output map (IO-map). This IO-map permits to determine the appropriate command signal $U$ to apply to the servovalve in order to obtain a desired mass flow rate entering each chamber, knowing its own internal pressure. An example of such an IO-map is shown in Fig. 4 for chamber N. Abry *et al.* introduced in [17] an algorithm to determine which command $U$ should be sent to a unique

[1]5/2 means two dependent controlled air outputs

5/2 servovalve connected to both cylinder chambers in order to directly get the appropriate $q_{mA}$ value.

Starting from this model, four error signals are created and used for control purposes. These error signals allowed Abry *et al.* [14] to propose a simple Lyapounov function to prove the stability of the control law.

$$\begin{cases} z_1 &= y - y_d \\ z_2 &= v - v_d + C_1 \cdot z_1 \\ z_3 &= F_{pneu} - F_d \\ z_{3i} &= \int z_3 \mathrm{d}t \end{cases} \qquad (6)$$

The "d" subscript indicates a desired value, so let $y_d$ be the desired position, $v_d$ its first derivative and $F_d$ the desired pneumatic force. The $z_{3i}$ error signal helps for the position control to get rid of any static error by adding an integral action. It is not compulsory but it does smooth the behavior of the interface.
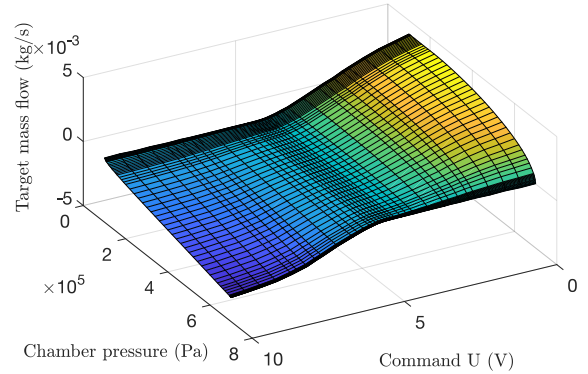


Figure 4: Servovalve Input-Output map, indicating the command level $U$ to apply to the servovalve in order to get a desired mass flow rate in chamber N knowing its internal pressure

### 2.2. Control laws

In this setup, $q_{mA}$ is used to control the pneumatic force or the position of the piston according to the system state. This section first details the position control, then focuses on the force control. In order to control the behavior of the pneumatic cylinder, a backstepping approach was chosen instead of linear approaches such as PID for the following reasons. First, concerning the force control that allows for a precise and customisable haptic experience, a classic PID controller did not produce satisfactory results. In this context, the force applied by the user can be considered as a disturbance to be rejected in order to produce the appropriate plunger reaction force. In practice, one could not obtain a fast enough rejection of this disturbance force with a PID control law. This is due to the absence of control of the pressure levels in the chambers and the non-linearities in the process (as visible in Fig. 4 and Equation (1)). The use of a backstepping approach allowed to tackle these two issues at once, thanks to a precise model. Finally, concerning the position control, a backstepping

approach also allows us to control the closed loop stiffness which has a major impact on the haptic feel produced by the cylinder [13].

The global control architecture is illustrated in Fig. 5, displaying both control laws as well as the switching algorithm.
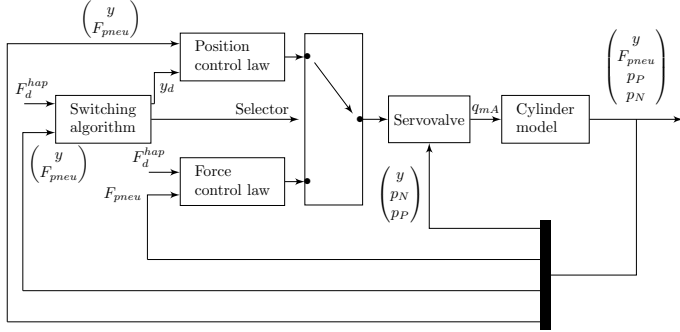


Figure 5: Control architecture of the syringe simulator

The control laws presented here were already discussed in [9, 14, 16]. They provide the basis for the design of the switching algorithm.
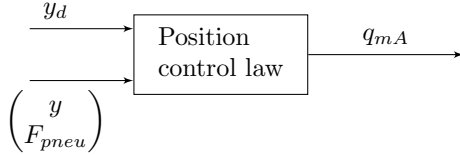
### 2.2.1. Position control



Figure 6: Block diagram of the position control law.

To use the position control, one has to set a reference trajectory $y_d$, generate its derivatives $v_d$, $a_d$ and $j_d$ and finally define the value for $F_d$, according to Abry *et al.* [14], using:

$$F_d = M \cdot (a_d + z_1 \cdot (C_1^2 - 1) - z_2 \cdot (C_1 + C_2)) + b \cdot v \quad (7)$$

For this control law, $q_{mA}$ can be defined as such, using the backstepping approach proposed by Abry *et al.* [14]:

$$q_{mA} = f_0 + f_1 \cdot z_1 + f_2 \cdot z_2 + f_3 \cdot z_3 + f_{3i} \cdot z_{3i} \quad (8)$$

with:

$$
\begin{aligned}
f_0 &= \frac{M^2 \cdot j_d + M \cdot K_{pneu} \cdot v - v \cdot b^2 + F_{pneu} \cdot b}{M \cdot B_1} \\
f_1 &= -\frac{M \cdot (C_1^3 - 2 \cdot C_1 - C_2)}{B_1} \\
f_2 &= \frac{M^2 \cdot (C_1^2 + C_1 \cdot C_2 + C_2^2 - 1) - 1}{M \cdot B_1} \\
f_3 &= -\frac{C_1 + C_2 + C_3}{B_1} \\
f_{3i} &= \frac{K_i}{B_1}
\end{aligned}
$$

In these expressions, $j_d$ is the desired jerk and $C_1$, $C_2$, $C_3$ and $K_i$ are constant positive parameters. $C_1$ and $C_2$ can be adjusted to control respectively the closed loop damping and the stiffness of the control law, as suggested in [14]. The closed loop stiffness can then be defined as $K_{cl} = M \cdot (C_1 \cdot C_2 + 1)$ and the closed loop damping as $B_{cl} = M \cdot (C_1 + C_2)$. These two physical parameters help to figure out the influences of each parameter. They can be tuned to get the desired haptic feel. This law allows the system to stabilize the piston at a desired position $y_d$ by leading all the errors defined in (6) to 0. The asymptotic stability has been proven in [14].
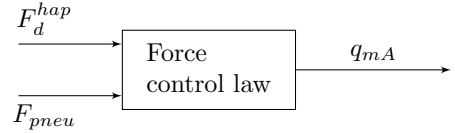
### 2.2.2. Force control



Figure 7: Block diagram of the force control law.

Concerning the pneumatic force control law, $q_{mA}$ is defined using the approach proposed in [9]:

$$q_{mA} = \frac{1}{B_1} \left( K_{pneu} \cdot v + \dot{F}_d^{hap} \right) - C_4 \cdot z_3 \quad (9)$$

where $C_4$ is a stricly positive constant parameter. It is designed using a backstepping approach on the last line of the equation set (1). This law allows the system to set the pneumatic force to a desired force $F_d^{hap}$. In this case, the control law does not include the integral state $z3i$ as the static error obtained was not too important for this study. Indeed to generate precise haptic feel, the dynamic of the force trajectory was the first concern. Its asymptotic stability has been proven in [9].

5

## 3. Replicating a syringe behavior

In this section, aforementioned models and control laws are used to turn a pneumatic cylinder into a pneumatic haptic interface. To do so, a supervisor controller monitors the switching between position (8) and force control (9) laws. First the global stability is considered. Then the switching behavior is described.

### 3.1. Stability analysis

The position and force control laws are independently stable. The issue addressed here concerns the stability of the global system. Once each control law is applied to the system, the dynamics become:

$$\begin{cases} \dfrac{\mathrm{d}z_1}{\mathrm{d}t} &= -C_1 \cdot z_1 + z_2 \\ \dfrac{\mathrm{d}z_2}{\mathrm{d}t} &= -z_1 - C_2 \cdot z_2 + \dfrac{z_3}{M} \\ \dfrac{\mathrm{d}z_3}{\mathrm{d}t} &= -\dfrac{z_2}{M} - C_3 \cdot z_3 \end{cases} \quad (10)$$

when the position control is active, and

$$\begin{cases} \dfrac{\mathrm{d}y}{\mathrm{d}t} &= v \\ \dfrac{\mathrm{d}v}{\mathrm{d}t} &= \dfrac{-b \cdot v + F_{pneu}}{M} \\ \dfrac{\mathrm{d}z_3}{\mathrm{d}t} &= -C_4 \cdot B_1 \cdot z_3 \end{cases} \quad (11)$$

when the force control is active.

Both control laws have their own asymptotic stability. Hence, in order to ensure the stability of the switched system, the dwell time of each law is considered. We determined a minimum duration to wait before next switching, which enables the system internal states to reach steady values. Concerning the position control, the average dwell time of each error signal [18] has to be considered. This average dwell time is provided by the eigenvalues of:

$$\mathbf{A}_1 = \begin{pmatrix} -C_1 & 1 & 0 \\ 1 & -C_2 & 1/M \\ 0 & -1/M & -C_3 \end{pmatrix} \quad (12)$$

Concerning the force control, we only have to consider the dynamics of $z_3$ given by:

$$\frac{\mathrm{d}z_3}{\mathrm{d}t} = -C_4 \cdot B_1 \cdot z_3 \quad (13)$$

As they are the only controlled dynamics, they can also be written as follows:

$$\mathbf{A}_2 = \begin{pmatrix} -C_4 \cdot B_1 & 0 & 0 \\ 0 & -C_4 \cdot B_1 & 0 \\ 0 & 0 & -C_4 \cdot B_1 \end{pmatrix}, \quad (14)$$

knowing that $z_1$ and $z_2$ are irrelevant during this phase and may be set to zero. Given that, each of these dynamics are asymptotically stable. Hespanha *et al.* [18] ensures that there exists a dwell time $\tau_D$ preventing the system to reach a chatter bound. We only have to ensure the system remains in a steady state for at least $\tau_D$. $\tau_D$ depends on the values of $C_1$, $C_2$, $C_3$, and $C_4$, and the desired stability margin. The values of $\tau_D$ are provided later on in section III.

It has to be noted that some dynamics remain uncontrolled in each law. For example, the position control law, in this configuration with only one servovalve, does not control the dynamics of $K_{pneu}$. However taking care of the asymptotic stability of the system appears to provide satisfying results (see [9, 17]).

Another approach would have consisted in using Fuzzy Logic (FL) [19, 20]. Yet another approach could be using the Filippov solutions [21]. The team not having skills in FL and as the current solution provides satisfactory results, these option have not been investigated further.

### 3.2. Switching Logic

As the objective is to simulate a syringe which can either keep a set position or render a desired resistance force to the user through the plunger flange, the supervisor algorithm must "guess" which control law has to be selected. Therefore, a triggering signal had to be defined to allow the system to use either one or the other control law depending on the situation. Throughout this paper, the piston position $y$ is considered rather than the plunger flange's one as both work together.

First, the algorithm starts with a position control placing the rod fully extended (see Fig. 8). Once initialized properly, the supervisor decides whether to use a position or a force control law anytime. This section describes the setting up of the algorithm step by step, showcasing how it works with some simulated examples. For these examples, the model (1) was simulated and a disturbance force was applied by a virtual user: a filtered step signal with a slight random part to be close to a real use case.
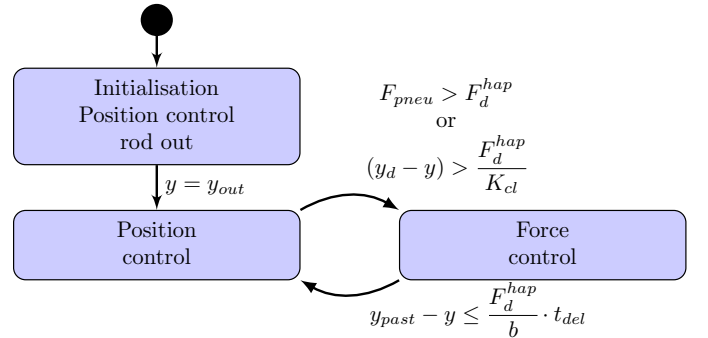


Figure 8: State diagram governing the control law switching

### 3.2.1. Switching from position to force control

If the active law controls the position, the algorithm checks whether the current pneumatic force created by the cylinder is greater than the current desired force ($F_{pneu} \geq F_d^{hap}$) or whether $(y_d - y) > \Delta y_{p \to f}$ where $\Delta y_{p \to f} = \dfrac{F_d^{hap}}{K_{cl}}$. If so, the algorithm selects the force control law. The condition $F_{pneu} \geq F_d^{hap}$, allows for a smooth switching from a position to a force control in terms of haptic cues, with minimal (if not absent) kicks. The condition $(y_d - y) > \Delta y_{p \to f}$, checks whether the plunger flange has been shifted enough from the equilibrium position. Indeed, when the position control law is active, the cylinder works as if there were a spring holding it to the equilibrium position with $K_{cl}$ as stiffness. So when the error between the equilibrium position and the current position exceeds $\Delta y_{p \to f}$, then the pneumatic force should be close to the desired force. This condition acts as a security as it is redundant with $F_{pneu} \geq F_d^{hap}$. It is useful when the plunger flange is shifted too quickly from the equilibrium position. Also, it should prevent some potential wind up of the integral action used for the position control.

As an example, Fig. 9 illustrates how the use of this trigger prevents the system from remaining in the position control too long, while limiting the spikes in the force signal.
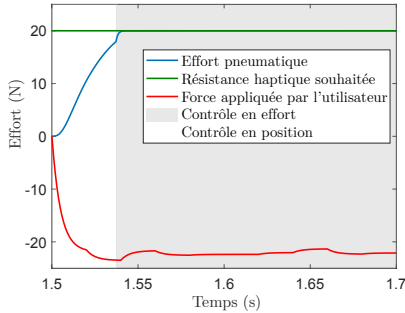


Figure 9: Simulated disturbance force, pneumatic force, and desired force. In this case the position based condition triggered first at t≈1.55 s creating a small rise in pneumatic force

### 3.2.2. Switching from force to position control

When the force control is active the equation of the state of the pneumatic cylinder is as follows:

$$\begin{cases} \dfrac{dy}{dt} = v \\[2mm] \dfrac{dv}{dt} = \dfrac{-b \cdot v + F_d^{hap}}{M} \end{cases} \qquad (15)$$

In this case, the backstepping controller acts so that the current pneumatic force is equal to the desired force. For demonstration purposes, $F_d^{hap}$ is considered constant and the flange is immobile at the start. First, the focus is on the triggering condition detecting that the user stopped pushing on the plunger flange. To be sure the condition will be triggered, it is recommended to use a low expected value of $F_d^{hap}$. Indeed, when the user stops pushing on the plunger flange, the initial velocity is then 0 as the plunger flange starts moving backward and the initial position is recorded as a set point. The flange velocity is then (by integrating the linear differential equation (15)):

$$v(t) = \frac{F_d^{hap}}{b} \cdot (1 - e^{-\frac{b}{M} \cdot t}) \qquad (16)$$

which then leads to:

$$y(t) - y_0 = \frac{F_d^{hap}}{b} \cdot (t + \frac{M}{b} e^{-\frac{b}{M} \cdot t}) \qquad (17)$$

At this point, when a switching is detected, $y_0$ then becomes $y_d$, the new equilibrium position, namely the position at which the user stopped pushing. So, after $t_{del}$ the plunger flange has moved as follows:

$$y_{past} - y_d = \frac{F_d^{hap}}{b} \cdot (t_{del} + \frac{M}{b} e^{-\frac{b}{M} \cdot t_{del}}) \qquad (18)$$

which can be simplified to:

$$y_{past} - y_d = \frac{F_d^{hap}}{b} \cdot t_{del} \qquad (19)$$

if $\frac{M}{b}$ is very small in comparison to $t_{del}$. Then, to detect a necessary switching from force control to position control, $(y(t) - y_d)$ has to be less or equal to $\Delta y_{f \to p} = \frac{F_d^{hap}}{b} \cdot t_{del}$.
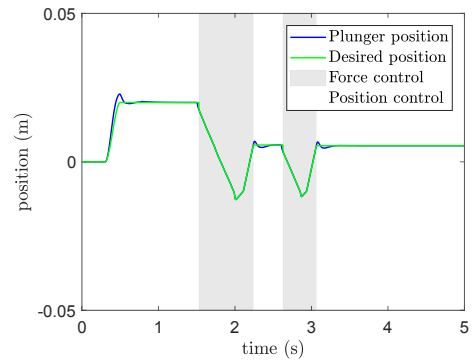


Figure 10: Simulated real position and desired position with a too severe condition to switch from force to position control. As a result, the algorithm did not detect the need to switch after $t \approx 3$ s and is too slow when $t \approx 2$ s

If this condition is overlooked, the worst case scenario may end up not detecting some necessary switching as shown in Fig. 10 at $t \approx 3$ s. To illustrate this scenario, the trigger level is arbitrarily set too high. Indeed the pneumatic force being quite low at this point, the plunger

flange did not move fast enough to trigger the condition. However, choosing a trigger value very close to 0 is particularly dependent on the hardware and the sensors. Thus one needs to be careful not to reduce the delay ($t_{del}$) too much as it would require a very precise position sensor.

### 3.2.3. Managing the switching

The role of the supervisor is to maintain the system stable but also to perform soft switching between control laws in order to render correct haptic cues. To prevent the supervisor to switch between both laws too frequently, a timeout signal is added to embed an hysteresis behavior as follows: the supervisor first checks the presence of a non null value of the timeout signal to determine whether a switching happened recently. If not, the algorithm looks whether one of the aforementioned switching conditions (depicted in Fig. 8) are true.

In Fig. 11 once the algorithm switches from force control to position control (at $t \approx 3$ s), as the desired force $F_d^{hap}$ is relatively small, the pneumatic force remains above $F_d^{hap}$. So, as $F_{pneu} \geq F_d^{hap}$ the algorithm switches back to force control. Then, the system alternates extremely rapidly between the two control laws for about 0.1 s until the system stabilize itself. Notice that it is a simulated case; this does not guarantee that the real system would also stabilize itself. From all those conditions, the final complete switching algorithm is illustrated as a flowchart in Fig. 12.

### 3.3. Validation through computer simulations

The aforementioned parameters, equations, model, and control laws are implemented in a Simulink® program depicted as a block diagram in Fig. 5. The feedback signal connecting the pneumatic cylinder output to the servovalve block highlights the need for a servovalve characterization in a real application for better performance. The simulation depicts a simple but realistic behavior. A noise was simply added to the applied force to take into account that the user does not apply a perfectly constant force on the plunger flange.

Results are shown in Fig. 13, where force and position are shown respectively in subfigure 13b and 13a. At first the algorithm activates the position control law, and when the user applies a force, at $t = 1.5$ s, the plunger flange starts moving away from the current equilibrium position, thus creating a pneumatic force (in blue in Fig. 13b) opposed to the user force. When this pneumatic force reaches the current desired force, the force control law takes place and keeps the pneumatic force at the desired value. At $t = 2$ s the user stops pushing on the flange and one can observe the switching from the force control to the position control at $t = 2.1$ s. During the short period when $2 < t < 2.1$ s, the plunger flange goes about 3 mm back
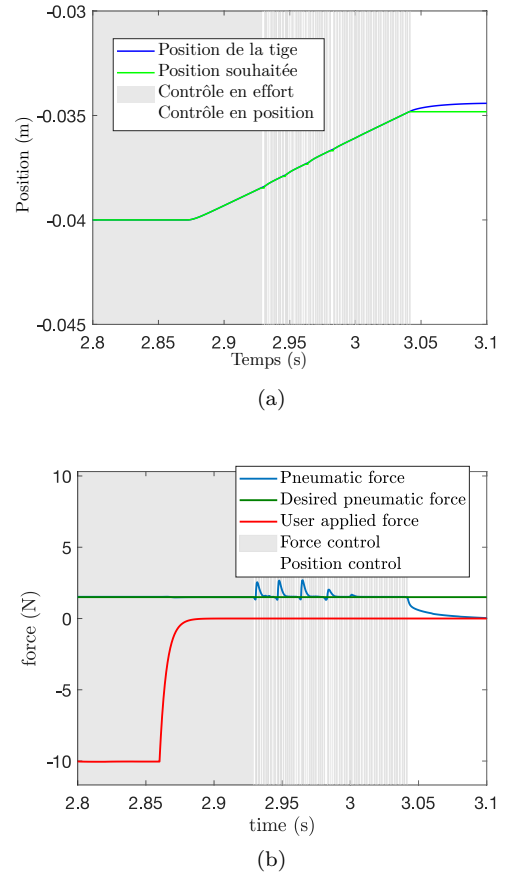


(a)



(b)

Figure 11: Simulation of switching using no timeout signal;(a) depicts respectively plunger flange real and desired position, (b) depicts user applied force, pneumatic force recorded, and desired force.

and then stops when the algorithm has detected that the plunger flange has moved in the opposite direction for a long enough distance. This backing motion can be lessen by reducing the delay between $y$ and $y_{past}$ as long as it remains greater than the stability delay $\tau_D$ introduced in section 2.1.

Overall, this simulation provides satisfactory results as it presents negligible jumps in pneumatic force and the backing motion remains quite small when the user stops applying force on the plunger. Our algorithm is able to produce smooth enough haptic cues while detecting the backing motion efficiently.

### 3.4. Conclusion from simulations

These computer simulations showed that the behavior of a syringe could be reproduced with realism, by using a pneumatic cylinder equipped with only one servovalve, one position and two pressure sensors, no force sensor, and two control laws switched according to the provided algorithm. Finally, the algorithm works best when it needs to reproduce a force higher than 2 N, as the plunger flange must go backwards a bit during a short period of time to
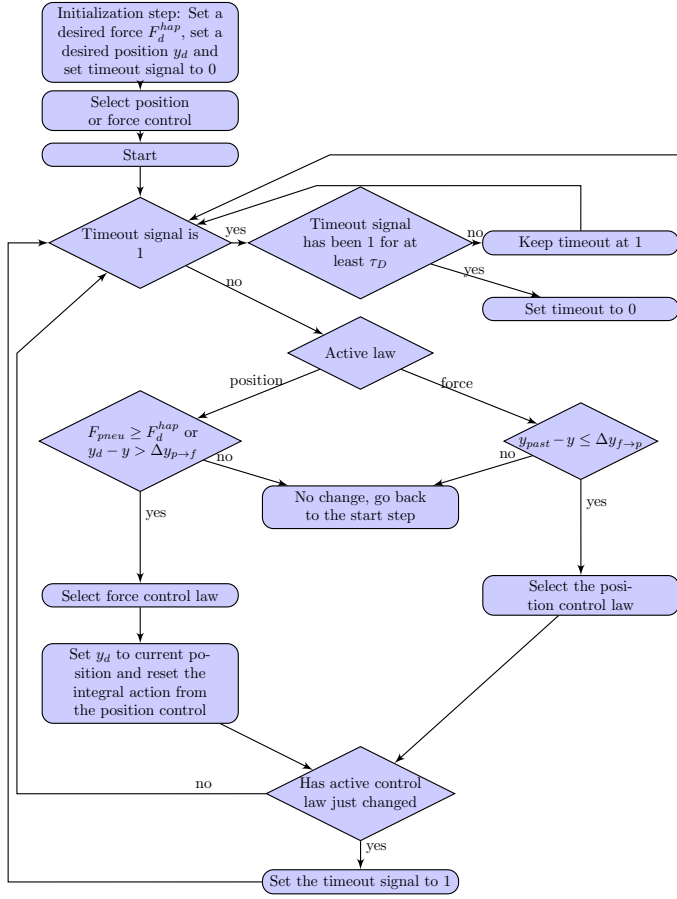
8

Figure 12: Switching algorithm flowchart.
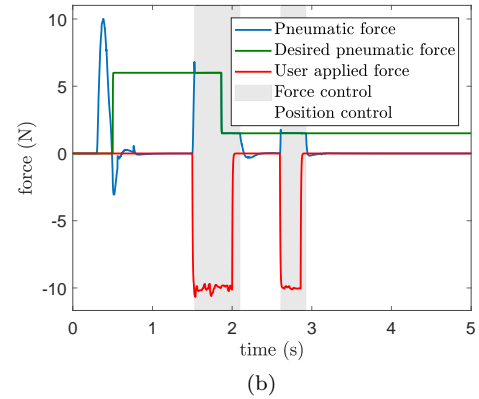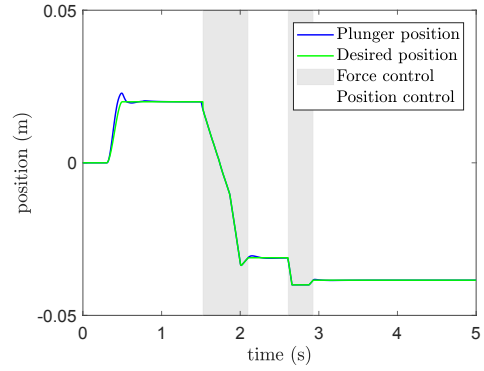


(a)



(b)

Figure 13: (a) Simulated position of the piston during a test involving user applied force (b) disturbance force, pneumatic force, and desired pneumatic force.

trigger a control law switch. In case someone wants to work with lower desired forces, the use of a small constant threshold for the conditions is recommended instead of $F_d^{hap}$. Moreover, it will be necessary to ensure that the integrator action, active during position control, is reset when this law is not activated.

## 4. Experimental validation

### 4.1. Test bench

The validation of the proposed controller for the syringe simulation application was performed on a separate test bench focusing only on the pneumatic LOR syringe simulation. This test bench features a double effect Airpel® low friction pneumatic cylinder (Airpel model M16D100D) coupled with a Festo MPYE®-5-M5-010 B servo-valve to control the air mass flow rates. This cylinder has a 16 mm diameter and a 100 mm stroke. The piston and shaft weigh $M \approx 60$ g. Two pressure transducers MEAS® U5136 and a low-friction linear variable differential transformer (LVDT) position sensor (DC-EC 2000 from Measurement Specialties) were used. The test bench used is visible in

Fig. 14. The control is performed on a dSPACE board (DS1103) running at a sampling rate of 1 kHz.

### 4.2. Parametrization

Compared to the aforementioned simulations, some compromises were made in order to respect some following constraints. Concerning the position control law, the performance had to be lowered to prevent instability. Indeed, in our case, asking for too quick a response in terms of positioning often resulted in a chattering behavior. This chattering greatly hinders the haptic feeling. Therefore, $K_i$ (the integral term of (8)) is kept at a low value: 10. Also, the algorithm was initialized with the force control active.

To effectively control the haptic feel produced by the interface, two cases have to be considered. First, when the position control law is active, it is necessary to set $B_{cl}$ and $K_{cl}$. Choosing a high value for $K_{cl}$ makes it harder to push the plunger flange away from its equilibrium position. In that case, the pneumatic force quickly reaches the desired force and the supervisor switches to the force control law at once. So one way to choose the value of $K_{cl}$ is to take into account the second condition which can also trigger
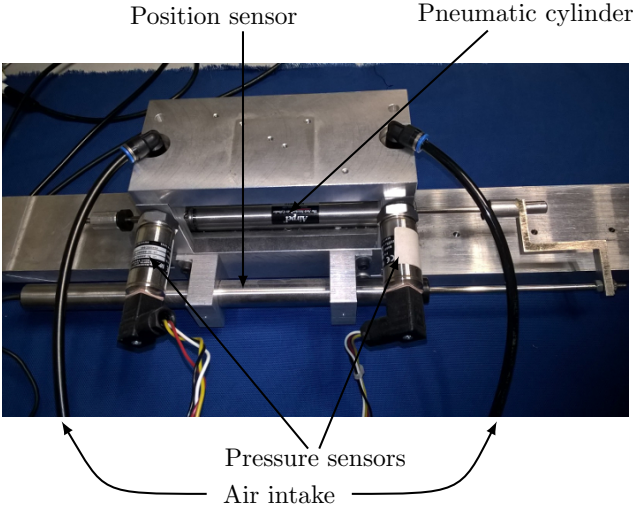
Figure 14: Test bench (the servovalve is not visible here).

this switching $((y_d - y) > \Delta y_{p \to f}$ with $\Delta y_{p \to f} = \dfrac{F_d^{hap}}{K_{cl}})$.

If the $F_{pneu} \geq F_d^{hap}$ condition gets triggered, the transition is the smoothest as the force control law is the closest to its equilibrium state. Concerning the $(y_d - y) > \Delta y_{p \to f}$ condition, the precision of the position sensor is important, because a high $K_{cl}$ would require a very small displacement to be considered as a triggering event. Therefore, $K_{cl}$ can be set *a priori* considering the desired displacement versus the desired force $F_d^{hap}$. For instance, a desired force of $F_d^{hap} = 10$ N and a 1 cm displacement as triggering event involve $K_{cl} = 1000$ N/m.

Knowing that the integral action ($z_{3i}$ in (8)), active during position control, increases the resulting pneumatic force, the precision of the position sensor may also be a limiting factor. Therefore, one should consider a larger[2] allowed displacement $\Delta y_{p \to f}$ and a lower closed loop stiffness $K_{cl}$. Values between 1000 and 2000 N/m should provide good performance for the position control law. Hence higher values of $K_{cl}$ generally result in a faster position control law. However choosing a relatively high $K_{cl}$ value may induce some undesired oscillations. Once $K_{cl}$ is set, it is necessary to do the same for $B_{cl}$. But, as suggested in [14], the system must comply with an additional condition in order to keep the stability of the position law:

$$B_{cl} \geq 2\sqrt{M \cdot (K_{cl} - M)} \qquad (20)$$

Here, choosing a value close to the minimal allowable value is preferable. Indeed, high closed loop damping generally adds some instability to the system. Also, in our application, motions being slow, the influence of $B_{cl}$ remains quite marginal, here $B_{cl} = 50$ N.s/m. The last parameter to set for the position control is $C_3$ which has to be set empirically through iterations. In our case $C_3 = 20$.

Finally, it is necessary to set the constant for the force control. This is also mostly done by iterations. In our case the value is $C_4 = 4 \cdot 10^{-4}$. Using these parameters guarantees $\tau_D \approx 0.1$ s according to Hespanha *et al.* [18].

### 4.3. Experimental results

The main objective of these experiments was to validate the realism of the rendered haptic cues of a LOR detection through the syringe with skilled users. A second objective was to assess the customization opportunities the system allows. The results are illustrated in Fig. 15 and Fig. 16.
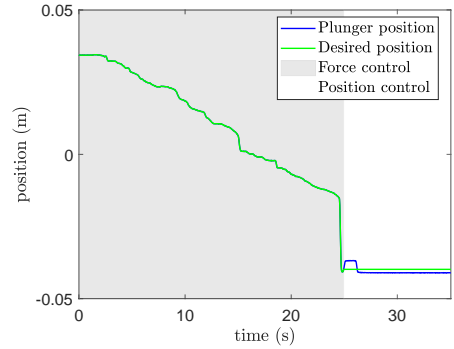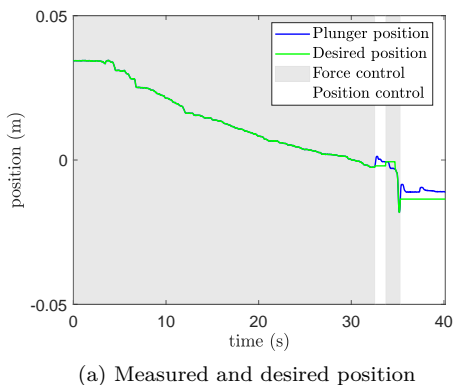


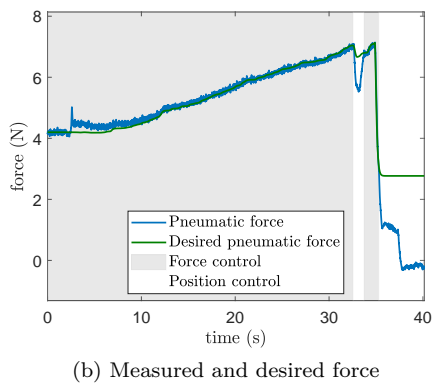(a) Measured and desired position
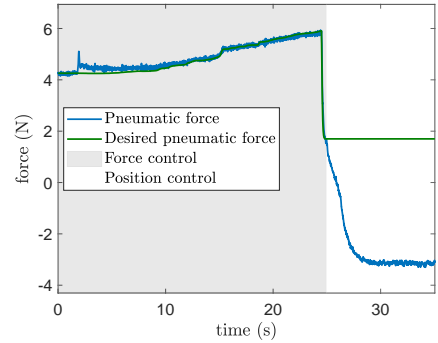


(b) Measured and desired force

Figure 15: Experimental results for an easy case: very sudden LOR, relatively low maximum force.

In the context of this paper, the system was tested without the needle insertion simulation, the virtual LOR position was set arbitrarily in the stroke of the cylinder flange around $y = -0.02$ m. Experiments were performed involving two anesthesiologists from *Hospices Civils de Lyon* in a context of epidural needle insertion simulation. These first trials were a way to asses the quality of the haptic rendering before integrating it into the complete simulator.

Three patient types corresponding to three increasing levels of difficulty were implemented here. The first level (Fig. 15) of difficulty consisted in a very sudden LOR and
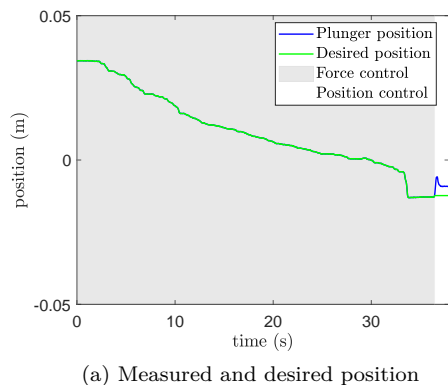
(a) Measured and desired position



(b) Measured and desired force

Figure 16: Experimental results for an intermediate case: sudden LOR, relatively high maximum force. This time showcasing the result of an hesitation by the user at $t \approx 35$ s.



(a) Measured and desired position



(b) Measured and desired force

Figure 17: Experimental results for an difficult case: smooth LOR, relatively high maximum force.
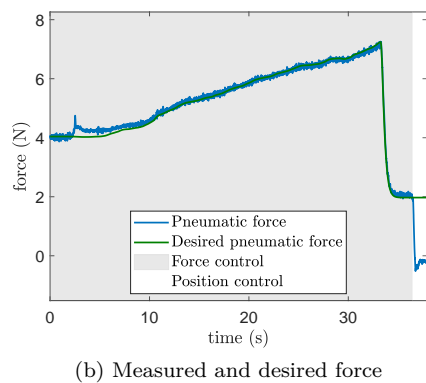
a relatively low maximum force corresponding to the injection of fluid in the derma. In the second level (Fig. 16, the maximum force was increased and the LOR was smoothed (a filtered step in this case). The increase of the maximum force is harder for the user as he has to be very careful not to miss the LOR point (which can be either subtle or very sudden). Concerning the LOR, softening the fall in resistance makes the LOR point more subtle and harder to be detected. The last level (Fig. 17), the maximum resistance was kept at a high level and the LOR was even smoother. This represents the most difficult case as making the LOR smoother makes it harder to detect. The parameters for these patients were based on feedback from the two professionals as well as on a study which published some measurement on forces during a LOR procedure [4].

### 4.4. Discussion

The results shown in the previous section as well as the feedback from the users are encouraging in terms of realism and efficiency of the LOR syringe simulator. Fig. 15 highlights a classical use of the interface with a constant pushing on the plunger all along the test. Fig. 16, in contrast, illustrates the switching during a test, with some hesitation at t ≈ 35 s. At this time, the user stopped pushing on the plunger before noticing a LOR to get a

better position. It is an interesting improvement over previous solutions, especially considering that it allows for a precise and deep customization of the haptic cues. Some of the presented results may include quick bursts in the plunger flange speed (t≈15 s in Fig. 15 for example) when the user pushes on it.

Concerning the realism of this LOR syringe simulator, both medical experts moderate their appreciation. Indeed, as the experiments were performed without any needle insertion, the difficulty of the procedure was greatly decreased as they could focus on only one task. In practice, the LOR is not only felt through the plunger flange but also through the needle insertion, the absence of the needle part might blur the perception of the users. According to these experts, it is difficult to fully separate the forces applied on the plunger flange from the needle insertion forces.

In the complete simulator, a new cylinder will be used, with less friction. This will thus allow smoother displacements. Also, instead of a arbitrary force trajectories, different flange resistant force levels will have to be set when the needle crosses each physical layer (outside, derma, supraspinous ligament, intraspinous ligament, ligamentum flavum, epidural space, dura, and muscles) as the leak of liquid in the real LOR syringe depends on the physiological

response of these body parts.

## 5. Conclusion

This paper introduces a control framework to render haptic cues by mean of a pneumatic cylinder. It can be especially used to simulate the LOR effect in an epidural needle insertion procedure. For this kind of application, compared to existing solutions [5, 6, 7, 8], two skilled anesthesiologists confirmed a good realism. Moreover, its customisability enables simulations of a wide range of difficulty levels, hence proposing a large improvement margin for the trainees. This simulator has been validated both in simulation and experimentally providing satisfactory results in regards to the stability of the system and the quality of haptic cues generated. Future directions will consist in updating the model of pneumatic cylinder to reduce its friction, as its actual friction level may mislead users.

On the complete simulator, featuring both a needle to insert and the LOR syringe, the LOR syringe simulation will be synchronized with the needle insertion haptic simulation providing hands-on training of the whole epidural needle insertion procedure. This should permit to efficiently and safely train and assess novice anesthetists skill on the complete gesture.

## ACKNOWLEDGMENT

## References

[1] N. Vaughan, V. N. Dubey, M. Y. Wee, R. Isaacs, A review of epidural simulators: Where are we today?, Medical Engineering & Physics 35 (9) (2013) 1235–1250. doi:10.1016/j.medengphy.2013.03.003.
URL http://linkinghub.elsevier.com/retrieve/pii/S135045331300057X

[2] J.-C. Granry, M.-C. Moll, État de l'art (national et international) en matière de pratiques de simulation dans le domaine de la santé, Tech. rep., Haute Autorité de la Santé (HAS) (2012).

[3] T. R. Coles, D. Meglan, N. W. John, The Role of Haptics in Medical Training Simulators: A Survey of the State of the Art, IEEE Transactions on Haptics 4 (1) (2011) 51–66. doi:10.1109/TOH.2010.19.
URL http://ieeexplore.ieee.org/document/5453367/

[4] D. Tran, King-Wei Hor, A. Kamani, V. Lessoway, R. Rohling, Instrumentation of the Loss-of-Resistance Technique for Epidural Needle Insertion, IEEE Transactions on Biomedical Engineering 56 (3) (2009) 820–827. doi:10.1109/TBME.2008.2011475.
URL http://ieeexplore.ieee.org/document/4760227/

[5] V. Manoharan, D. van Gerwen, J. J. van den Dobbelsteen, J. Dankelman, Design and validation of an epidural needle insertion simulator with haptic feedback for training resident anaesthesiologists, in: Proc. of the Haptics Symposium (HAPTICS), 2012, IEEE, 2012, pp. 341–348.

[6] J. C. Magill, M. F. Byl, M. F. Hinds, W. Agassounon, S. D. Pratt, P. E. Hess, A Novel Actuator for Simulation of Epidural Anesthesia and Other Needle Insertion Procedures:, Simulation in Healthcare: The Journal of the Society for Simulation in Healthcare 5 (3) (2010) 179–184. doi:10.1097/SIH.0b013e3181ce761a.
URL https://insights.ovid.com/crossref?an=01266021-201006000-00009

[7] V. Dubey, N. Vaughan, M. Y. K. Wee, R. Isaacs, Biomedical Engineering in Epidural Anaesthesia Research, in: A. Andrade (Ed.), Practical Applications in Biomedical Engineering, InTech, 2013. doi:10.5772/50764.
URL http://www.intechopen.com/books/practical-applications-in-biomedical-engineering/biomedical-engineering-in-epidural-anaesthesia-research

[8] D. Thao, A. T. M, S. M. A, Development and Evaluation of an Epidural Injection Simulator with Force Feedback for Medical Training, Studies in Health Technology and Informatics (2001) 97–102doi:10.3233/978-1-60750-925-7-97.
URL http://www.medra.org/servlet/aliasResolver?alias=iospressISSNISBN&issn=0926-9630&volume=81&spage=97

[9] T. Senac, A. Lelevé, R. Moreau, Control laws for pneumatic cylinder in order to emulate the Loss Of Resistance principle, in: Proc. of the 20th World Congress of the International Federation of Automatic Control, Toulouse, France, 2017.
URL https://hal.archives-ouvertes.fr/hal-01506823

[10] M. Q. Le, M. T. Pham, M. Tavakoli, R. Moreau, Development of a hybrid control for a pneumatic teleoperation system using on/off solenoid valves, in: Proc. of the 2010 IEEE/RSJ International Conference on Intelligent Robots and Systems, 2010, pp. 5818–5823. doi:10.1109/IROS.2010.5650406.

[11] A. Talhan, S. Jeon, Pneumatic Actuation in Haptic-Enabled Medical Simulators: A Review, IEEE Access 6 (2018) 3184–3200. doi:10.1109/ACCESS.2017.2787601.

[12] M. Bouzit, G. Burdea, G. Popescu, R. Boian, The Rutgers Master II-new design force-feedback glove, IEEE/ASME Transactions on Mechatronics 7 (2) (2002) 256–263. doi:10.1109/TMECH.2002.1011262.

[13] N. Herzig, R. Moreau, T. Redarce, A new design for the BirthSIM simulator to improve realism, in: 2014 36th Annual International Conference of the IEEE Engineering in Medicine and Biology Society, 2014, pp. 2065–2068. doi:10.1109/EMBC.2014.6944022.

[14] F. Abry, X. Brun, S. Sesmat, E. Bideaux, Non-linear position control of a pneumatic actuator with closed-loop stiffness and damping tuning, in: Proc. of the 2013 European Control Conference (ECC), Zürich, Switzerland, 2013, p. 1089.
URL http://www.nt.ntnu.no/users/skoge/prost/proceedings/ecc-2013/data/papers/0463.pdf

[15] R. Park, Two reaction theory of synchronous machines, AIEE Transactions 48.

[16] N. Herzig, R. Moreau, T. Redarce, F. Abry, X. Brun, Nonlinear position and stiffness Backstepping controller for a two Degrees of Freedom pneumatic robot, Control Engineering Practice 73 (2018) 26–39. doi:10.1016/j.conengprac.2017.12.007.
URL http://www.sciencedirect.com/science/article/pii/S0967066117302812

[17] F. Abry, Contribution à la commande et l'observation des actionneurs électropneumatiques : de l'intérêt de la transformée A-T, Ph.D. thesis, L'institut national des sciences appliquées de Lyon (2013).

[18] J. P. Hespanha, A. S. Morse, Stability of switched systems with average dwell-time, in: Proc. of the 38th IEEE Conference on Decision and Control (Cat. No.99CH36304), Vol. 3, 1999, pp. 2655–2660 vol.3. doi:10.1109/CDC.1999.831330.

[19] J. Qiu, K. Sun, T. Wang, H. Gao, Observer-Based Fuzzy Adaptive Event-Triggered Control for Pure-Feedback Nonlinear Sys-

tems with Prescribed Performance, IEEE Transactions on Fuzzy Systems (2019) 1–1. `doi:10.1109/TFUZZ.2019.2895560`.
URL `https://ieeexplore.ieee.org/document/8626481/`

[20] K. Sun, S. Mou, J. Qiu, T. Wang, H. Gao, Adaptive Fuzzy Control for Non-Triangular Structural Stochastic Switched Nonlinear Systems with Full State Constraints, IEEE Transactions on Fuzzy Systems (2018) 1–1. `doi:10.1109/TFUZZ.2018.2883374`.
URL `https://ieeexplore.ieee.org/document/8544037/`

[21] A. F. Filippov, Differential equations with discontinuous right-hand sides, no. 18 in Mathematics and its applications Soviet series, Kluwer, Dordrecht, 1988, oCLC: 17549553.